ELSEVIER

Astroparticle Physics 18 (2002) 237–248

Astroparticle Physics

www.elsevier.com/locate/astropart

Geometry and optics calibration for air fluorescence detectors using star light

High Resolution Fly's Eye Collaboration

P.A. Sadowski [a,b], A.M. van der Zande [a,c], R. Abbasi [d], T. Abu-Zayyad [d], G. Archbold [d], J. Bellido [e], K. Belov [d], J.W. Belz [f], D.R. Bergman [g], J. Boyer [a], Z. Cao [d], R. Clay [e], B. Dawson [e], A.A. Everett [d], J.H.V. Girard [d], R.C. Gray [d], W.P. Hanlon [g], B.F. Jones [d], C.C.H. Jui [d], D.B. Kieda [d], K. Kim [d], B. Knapp [a], W. Lee [a], E.C. Loh [d], K. Martens [d], G. Martin [h], N. Manago [i], E.J. Mannel [a], J.A.J. Matthews [h], J.N. Matthews [d], J.R. Meyer [d], T. Minagawa [i], S.A. Moore [d], P. Morrison [d], A.N. Moosman [d], J.R. Mumford [d], L. Perera [g], K. Reil [d], R. Riehle [d], M. Roberts [h], M. Sasaki [h], M. Sasano [h], M. Seman [a], S.R. Schnetzer [g], P. Shen [d], K. Simpson [e], J.D. Smith [d], P.V. Sokolsky [d], C. Song [a], R.W. Springer [d], B.T. Stokes [d], M. Teshima [i], S.B. Thomas [d], G.B. Thomson [g], T.D. VanderVeen [d], S. Westerhoff [a,*], L.R. Wiencke [d], A. Zech [g], X. Zhang [a]

[a] *Department of Physics and Nevis Laboratories, Columbia University, 538 West 120th Street, New York, NY 10027, USA*
[b] *The University of Toledo, Toledo, OH 43606, USA*
[c] *University of California at Santa Cruz, Santa Cruz, CA 95064, USA*
[d] *Department of Physics and High Energy Astrophysics Institute, University of Utah, Salt Lake City, UT 84112, USA*
[e] *Department of Physics, University of Adelaide, Adelaide, SA 5005, Australia*
[f] *Department of Physics, Montana State University, Bozeman, MT 59717, USA*
[g] *Department of Physics and Astronomy, Rutgers University—The State University of New Jersey, Piscataway, NJ 08854, USA*
[h] *Department of Physics and Astronomy, University of New Mexico, Albuquerque, NM 87131, USA*
[i] *Institute for Cosmic Ray Research, University of Tokyo, Kashiwa City, Chiba 277-8582, Japan*

Received 4 December 2001; accepted 19 March 2002

Abstract

The high resolution Fly's Eye (HiRes) detector in Dugway, Utah, is an air fluorescence detector designed for the measurement of the energy and arrival direction of cosmic ray particles with energy $E > 10^{18}$ eV. HiRes monitors the night sky for fluorescence light from air shower cascades induced by cosmic ray primaries. The light is collected by mirrors and projected onto arrays of photomultiplier tubes that provide an image of the air shower.

* Corresponding author. Tel.: +1-212-854-3316; fax: +1-212-854-3366.
E-mail address: westerhoff@nevis.columbia.edu (S. Westerhoff).

PII: S0927-6505(02)00143-3

HiRes is an astronomical instrument, and the accuracy of the mirror pointing and understanding of the optical properties of the mirror–camera units is crucial. We present a method to cross-check and monitor the mirror pointing by using star light. A star crossing the field of view of a photomultiplier tube causes a temporary increase in the total light detected by the tube. Using UV bright stars, we analyze the pointing accuracy of the HiRes 2 detector, and evaluate the shape of a point-like object as a function of distance to the mirror axis.

PACS: 95.55.Vj; 95.45.+i; 95.85.Ry
Keywords: High Resolution Fly's Eye experiment; HiRes; Cosmic ray detector; Air fluorescence technique; Calibration; UV star light

1. Introduction

Several large experimental facilities are currently operating or being built to measure the flux and the arrival directions of ultra-high energy cosmic ray particles with energies above 10^{18} eV. Their origin and the mechanisms that accelerate them to these energies, the highest particle energies observed in the universe, are still unknown. A systematic mapping of the sky at EeV energies is likely to shed light on these important questions.

To first order the flux of cosmic ray particles above 10^{10} eV follows a power law in energy, $dN/dE \propto E^{-\gamma}$, with an overall γ of about 2.8. At energies above 10^{19} eV, the flux becomes so extremely low (0.5 $km^{-2}\,yr^{-1}\,sr^{-1}$) that balloon- or satellite-born experiments are no longer feasible. The large effective area necessary for a sufficient event rate requires earthbound experiments. Consequently, the high energy particle is detected indirectly as cosmic ray primaries entering the Earth's atmosphere interact with atmospheric nuclei to produce large cascades of relativistic secondary particles known as extensive air showers. Cosmic ray experiments are typically large, sparsely instrumented arrays of counters which measure the secondary particles reaching the ground, like the AGASA array [1] currently operating in Japan.

Alternatively, air fluorescence detectors exploit the fact that the particle cascade dissipates much of its energy while exciting and ionizing air molecules. The excited nitrogen molecules fluoresce in the near UV with an emission line spectrum where roughly 80% of the light is emitted between 300 and 450 nm. The fluorescence light is emitted isotropically and its intensity is proportional to the number of charged particles in the shower. Air fluorescence detectors consist of arrays of telescopes that image fluorescence light from distant air showers onto arrays of photomultiplier tubes. This technique requires detailed knowledge of atmospheric transmission of light and is presently restricted to operation on clear dark nights (about 10% of the "on time" of a ground array). It also requires a dry desert climate.

The air fluorescence technique was pioneered by the Fly's Eye experiment [2], which took data between 1981 and 1992 at the US Military's Dugway Proving Grounds in the Utah desert. HiRes, the high resolution Fly's Eye detector, is a larger successor of this experiment and operates at the same site.

At energies above 10^{20} eV, the Larmor radius of cosmic ray protons becomes sufficiently large for the primary cosmic ray particle to point back to within a few degrees of its origin. As an astronomical instrument, pointing accuracy is of crucial importance for HiRes. Unfortunately, there is no "standard candle" of ultra-high energy cosmic rays that could be used to check the pointing accuracy and evaluate the optical properties of the mirrors. We have to use indirect approaches instead.

In this paper, we describe methods for using stars for geometry calibration of air fluorescence detectors. While monitoring the night sky for UV light from distant air showers, HiRes is also sensitive to UV light from stars crossing the field of view. With their well-known position, orders of magnitude more accurate than the resolution of HiRes, and their point-like shape, stars are ideal tools to test the pointing of the detector and analyze the optical properties of the HiRes mirrors

and photomultiplier cameras. We also describe how stars are used to evaluate the *spot shape*, i.e. the shape of the image of a point-like object on the photomultiplier cluster.

The paper is organized as follows. After a description of the HiRes detector in Section 2, we outline in Sections 3 and 4 how star tracks are detected and identified. Section 5 describes how stars are used for an absolute check of the mirror pointing. In Section 6, the shape of the image of a star on the camera cluster is analyzed. Section 7 summarizes the results.

2. The HiRes detector

HiRes is an air fluorescence experiment with two sites (HiRes 1 and 2) at the US Military's Dugway Proving Ground in the Utah desert (112° W longitude, 40° N latitude, vertical atmospheric depth 860 g/cm^2). The two sites are separated by a distance of 12.6 km which allows "stereoscopic" observation of air showers. This leads to a more precise geometrical reconstruction than "monocular" mode. HiRes is sensitive to showers with energies above 10^{18} eV.

Each of the two HiRes "eyes" comprises several telescope units monitoring different parts of the night sky. With 22 (42) telescopes with 256 photomultiplier tubes each at the first (second) site, the full detector covers about 360° (336°) in azimuth and 3–16.5° (3–30°) in elevation above horizon. A telescope consists of a mirror for light collection and a cluster of photomultiplier tubes in the focal plane. The mirrors have a collection area of 4 m^2 and a radius of curvature R of 474 cm. The distance between the tube cluster and the mirror is set to $0.97(R/2)$. Since this is slightly out of focus, it increases the width of the spot shape for points at the center of the cluster, but it also makes the width of the spot shape more uniform across the cluster.

The photomultiplier tubes have flat hexagonal bialkaline photocathodes. The 256 tubes of each camera are arranged in a hexagonal pattern of 16 columns and 16 rows with a center-to-center distance between neighboring tubes of 4.18 cm. Each tube has a field of view of $1° \times 1°$. The photomultiplier tubes are enclosed in a cluster box with a glass filter which transmits in the near UV and reduces the contamination of the signal by night sky background and artificial light sources.

The fluorescence light generated by the passage of an air shower is viewed by a succession of photomultipliers. Each photomultiplier detects light from a small part of the shower trajectory. The arrival direction of the primary cosmic ray can then be determined by reconstructing the trajectory using the photomultiplier pointing directions and triggering times. The number of fluorescence photons detected along the shower trajectory allows the reconstruction of the longitudinal development profile of the shower, including $X_{\max}$, the position of the shower maximum in the atmosphere. $X_{\max}$ is an indicator of the chemical composition of the incoming cosmic ray flux because heavier nuclei induce earlier shower development.

The HiRes 2 site differs in that the HiRes 1 sample-and-hold system is replaced by an FADC system which continuously digitizes the photomultiplier signals at 10 MHz by 8-bit FADCs. This system uses small commercial 24-bit digital signal processors (DSPs) which, among other tasks, carry out trigger formation and basic monitoring. It is described in detail in [3]. Fig. 1 shows the basic principle: a shower signal appears as light sweeping across the cluster appearing in one analog sum while disappearing from a neighboring sum. The tubes are operated with the photocathode at

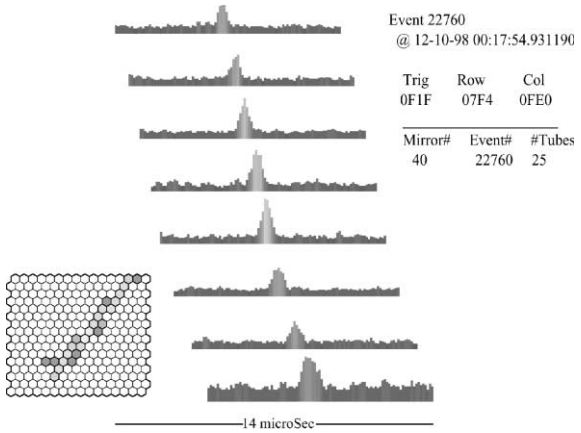

Fig. 1. HiRes 2 event display of a cosmic ray shower with FADC profiles for eight viewing channels [3].

ground potential, so the anode signals are AC coupled and appear as small fluctuations in the 1 kV anode high voltage.

HiRes 2 can detect showers as far away as 60 km. A typical shower is seen in 10–100 tubes. Depending on the distance to the detector and the energy of the shower, a tube signal lasts from 0.1 to 4 μs and ranges from a few to several thousands of photoelectrons. The typical night sky noise on dark clear nights is 20–40 photoelectrons/μs/tube.

The HiRes 2 detector has the capability of taking so-called pedestal snapshots. They allow the monitoring of drifts in the background light seen by each tube, for example caused by changing weather conditions or light sources (stars, planets) crossing the field of view. Snapshots are taken automatically with no trigger requirement at fixed intervals 4.8 times/s. No raw data is stored for snapshots. Instead, we average the mean and the variance for all measurements within a 25 μs time window, and report and store the average of 48 windows for each tube every 10 s.

A star crosses the field of view of a tube in about 4 min. Because the anode signal is AC coupled with a time constant of 500 μs, slow changes in the ambient light level like the drift caused by a star will be filtered and can not be observed in the *mean* of the snapshot measurements. However, an increase in the night sky background or a bright star in the field of view of a tube leads to additional noise and therefore to an increase in the statistical fluctuations, i.e. the *variance*, of the measurement. The variance therefore provides an indirect tool to determine the ambient light level or the number of arriving photons. Its actual value is approximately equal to the number of photoelectrons in 100 ns, so for the typical night sky noise the variance is 2–4 photoelectrons.

The signal of a star in the snapshot data has a typical shape as shown in Fig. 2. Depending on the brightness of the star, peak values for the variance range from 5 up to 50 photoelectrons over a background of 2–4 photoelectrons. As an example, Lambda Scorpio in Fig. 2, with a visible magnitude of 1.6 and a flux of 5.1×10^{-9} erg cm^{-2} s^{-1} Å^{-1} at 2740 Å [4], has an intensity of about 14 photoelectrons in 100 ns at the peak, i.e. when its image is at the center of the photomultiplier. In comparison, a typical airshower produces several hundreds of photoelectrons per tube near the shower maximum, but the air shower signal comes as short pulses of μs duration.

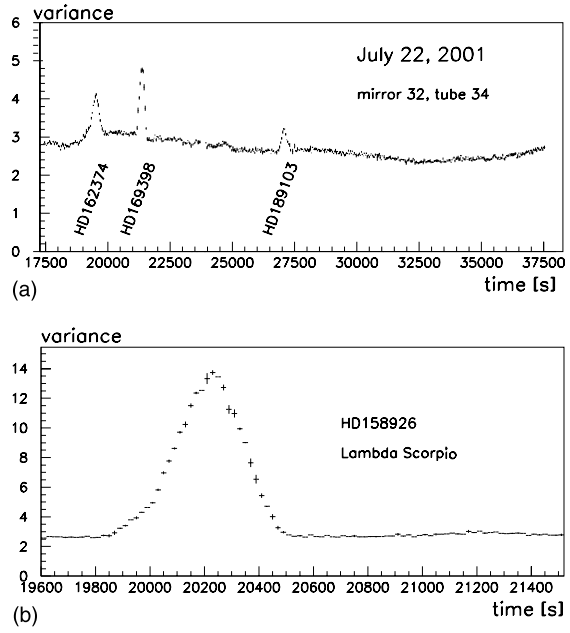

Fig. 2. (a) HiRes 2 snapshot data taken over the course of a night for one of the photomultiplier tubes ($1^\circ \times 1^\circ$ field of view). (b) Shape of the signal (variance vs. time) for the bright star Lambda Scorpio.

3. The signal

The challenge is to find the signature of a star in the presence of a slowly varying night sky background and sharp peaks and edges caused by noisy electronics. For an efficient detection of a star transit with minimal contamination by "fake" events, we can make use of the very distinct duration and (roughly Gaussian) shape of a star transit.

We use the second-derivative method as described in detail in [5]. It is a very general and typically very fast method to search for peaks on a slowly varying (linear) background. The basic idea is that the second derivative is non-zero only in the neighborhood of a peak. Taking the second-derivative eliminates linear changes in the back-

ground rate and produces a distinct signature for a Gaussian-shaped signal. In our case, the snapshot data is given for discrete times t_i, so we replace the second derivative by the *second difference* S_i, which is given for each time bin i as

$$S_i = N_{i+1} - 2N_i + N_{i-1}, \tag{1}$$

where N_i is the variance for the snapshot data taken at time t_i. Like the second derivative, this should be non-zero only in the vicinity of the peak. In practice, N_i has a statistical error which makes S_i fluctuate, and without further smoothing of the signal, S_i is comparable to its standard deviation

$$P_i = \sqrt{N_{i+1} + 4N_i + N_{i-1}} \tag{2}$$

even for strong peaks. As suggested in [5], we reduce the standard deviation of S_i by averaging over neighboring time bins with a smoothing window of width $w = 2m + 1$,

$$S_i = \sum_{j=i-m}^{i+m} S_j. \tag{3}$$

This procedure is repeated z times. For a given application and a given shape and width of the signal, the parameters z and w have to be chosen so that the sensitivity of the method is maximized. Typically, the optimal smoothing window w is of the order of the width of the signal, so the method is ideally suited to preferentially pick out peaks of a given length and discriminate against peaks of different duration.

Computationally, this method comes down to the calculation of the *weighted average*

$$S_i(z, w) = \sum_j C_{ij}(z, w) N_j \tag{4}$$

of the data points N_j with weight factors C_{ij} given recursively by

$$C_{ij}(z, w) = \sum_{j=i-m}^{i+m} C_{ij}(z-1, w), \tag{5}$$

and

$$C_{ij}(0, w) = \begin{cases} 0 & \text{if } |j-i| \geqslant 2 \\ 1 & \text{if } |j-i| = 1 \\ -2 & \text{if } j = i. \end{cases} \tag{6}$$

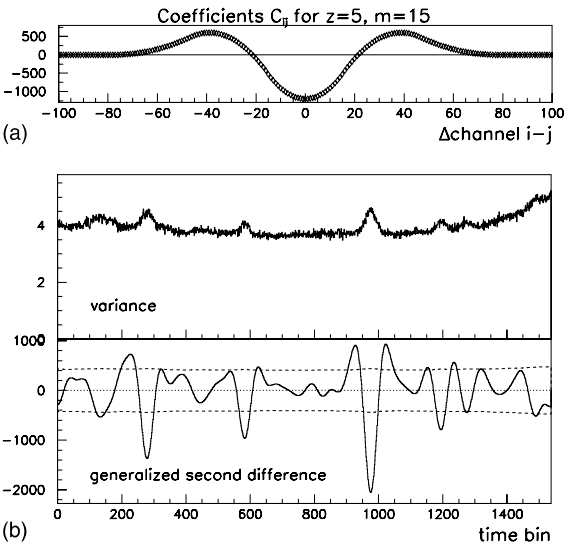

Fig. 3. (a) Coefficients C_{ij} for calculating the generalized second difference for the photomultiplier tube variances vs. time. (b) shows the variance and the generalized second difference as a function of time for a typical tube during the course of a night. A time bin corresponds to one snapshot and therefore approx. 10 s. The dashed line indicates the 1σ error band.

For the specific application of this paper, we find that $m = 15$ and $z = 5$ maximizes the sensitivity. Fig. 3(a) shows the resulting C_{ij} and Fig. 3(b) shows the data points and the generalized second difference for a photomultiplier tube on a day with large fluctuations of the ambient light level. The 1σ error band is indicated by the dashed lines.

The advantages of this methods are twofold. The second-derivative eliminates all linear changes in the variance, which takes care of the slow changes in the ambient night sky light level as for example caused by clouds. Since the method requires us to optimize the parameters z and w, it increases the purity of the detection by making explicit use of the shape and duration of the signal. The typical shape of the second derivative of a Gaussian signal helps to discriminate against non-Gaussian changes in the variance (e.g. edges and sharp peaks). With choosing a smooth scale appropriate for the typical duration of a star transit, we can discriminate against changes in the variance on much shorter or much longer time scales.

4. Matching peaks and stars

The basis of the star search is the TD 1 Catalog of Stellar UV Fluxes [4], which is the result of a sky-scan experiment aboard the TD 1 satellite of the European Space Research Organization ESRO (now ESA). The TD 1 catalog contains the absolute UV flux of 31,215 stars in four pass-bands (1565, 1965, 2365, and 2740 Å). As HiRes works in the near UV, the flux at 2740 Å is the most relevant parameter. Peaks and stars are matched by comparing peak positions with stars within 2° of the equatorial coordinates of the tube at the peak time. If two or more stars are within this range, a matching decision is made based on the UV brightness and the angular distance between the star position and the sky coordinates of the center of the field of view of the tube.

Fig. 4(a) shows the sky coverage of the detector on a typical night in equatorial coordinates. HiRes can detect stars down to flux levels of approximately 10^{-11} erg cm^{-2} s^{-1} Å^{-1} with high efficiency. Fig. 4(b) shows the flux distribution (at 2740 Å) of all stars from the TD1 catalog as compared to the flux distribution (hatched) of stars that are detected by HiRes. Only stars which are in the field of view for more than 5 min and are detected by at least three tubes are considered for this plot.

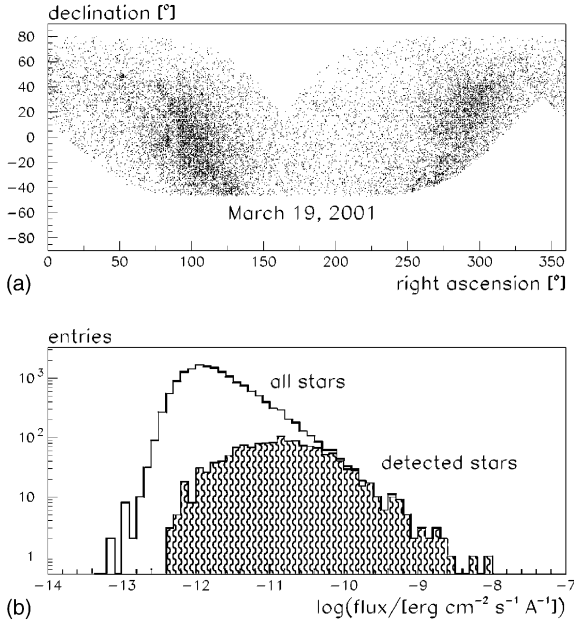

Fig. 4. Sky coverage on a typical night (19 March 2001): (a) position of all stars from the TD1 catalog in the field of view of HiRes in equatorial coordinates, (b) flux distribution of stars in the field of view, and detected stars (hatched).

Since the atmospheric extinction is larger for lower elevation, the upper ring of HiRes mirrors, covering elevations from 16.5° to 30°, is sensitive to fainter stars than the lower ring (3–16.5°). Fig. 4 reflects the average sensitivity of the rings.

On an average night with 6–8 h of observation time, around 600 stars are identified. The number of stars per mirror shows large variations from mirror to mirror. It ranges from 40 to a few, depending on the galactic coordinates covered by a particular mirror in the course of a night. As an example, Fig. 5(a) shows the tracks seen in mirror 2 within 8 h of data taking on 19 March 2001. Fig. 5(b) shows one track and the corresponding tube signals associated with the star track.

5. Geometry calibration

The first application of the star survey is a geometry calibration of the detector. A comparison of the actual pointing direction with the design value and a monitoring of the pointing accuracy over time with direct methods (theodolite,...) is tedious and time consuming. We need a tool for continuous monitoring of the geometry, as the mirror pointing may change slightly over several years of operation or over the course of a year. A slight overall deviation in altitude for example can be expected as the concrete foundations of the detector buildings settle.

The pointing accuracy of the HiRes 2 mirrors has been checked independently using star light observed by a CCD camera in turns mounted at the center of each mirror [6]. Compared to the direct measurement of stars with the photomultiplier camera as described here, the CCD method is sensitive to fainter stars as the light does not have to pass the UV filter. The advantage of the direct measurement of stars with the photomultiplier camera itself is that it provides a *continuous* geometry survey of *all* detector units, in principle on a nightly basis. If the method is applied over several

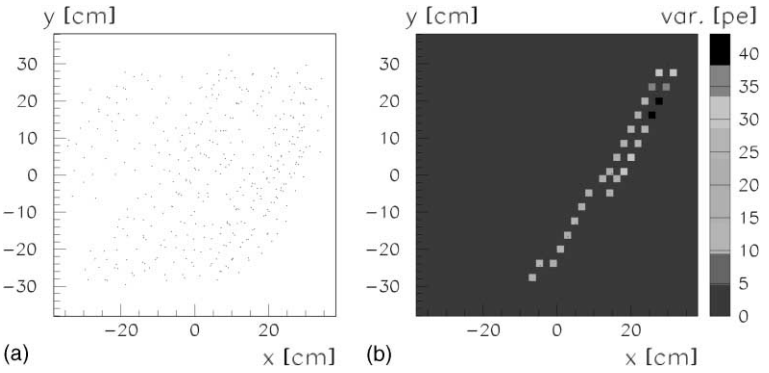

Fig. 5. (a) All star tracks observed in mirror 1 on 19 March 2001. (b) Typical star track with the color code indicating the maximum variance seen by the photomultiplier tubes along the track.

nights, it provides geometry monitoring and an overall geometry correction with high accuracy.

In the following analysis, we use a Cartesian coordinate system for each camera where the z-axis coincides with the mirror axis, the line from the center of curvature of the spherical mirror to the center of the photomultiplier camera. The xy-plane is the PMT camera plane, so x and y are the Cartesian coordinates of the tube centers with respect to the camera center. In terms of horizontal coordinates, x corresponds to azimuthal angles and y to elevation. The coordinates for stars in the field of view of a camera are transformed from their equatorial coordinates to tube cluster coordinates $(x_{\text{star}}, y_{\text{star}})$ for any given snapshot time. A star should be closest to the center of the tube when the signal in the tube peaks. For every tube in which a star is identified, we calculate the distance between the center of the tube and the true position of the star image on the cluster at the time of the peak. The sum of the squares of all these distances for a given mirror is then minimized with a simple χ^2-minimization, where we allow the tube position to vary as

$$x_{\text{new}} = (1 + P_1)(x_{\text{tube}} \cos(P_2) - y_{\text{tube}} \sin(P_2)) + P_3 \tag{7}$$

$$y_{\text{new}} = (1 + P_1)(x_{\text{tube}} \sin(P_2) + y_{\text{tube}} \cos(P_2)) + P_4 \tag{8}$$

with four free parameters P_1 to P_4 in the χ^2-minimization. $(x_{\text{tube}}, y_{\text{tube}})$ are the start values for the tube position. The four free parameters have the following meaning. The first parameter P_1 is a scaling of the tubes away from the center of the tube cluster. To first order P_1 corrects for deviations in the radius of curvature of a mirror and for changes in the effective camera–mirror distance due to the treatment of the (flat) camera as a curved surface. The tilt parameter P_2 deals with rotation of the tube cluster around the mirror axis. The two offset parameters (P_3, P_4 for horizontal and vertical offset, respectively) deal with shifts in position of the entire cluster with respect to the mirror axis. The (corrected) tube position $(x_{\text{new}}, y_{\text{new}})$ is then given by the four parameters P_1 to P_4 which minimize

$$\chi^2 = \sum_i \left[(x_{\text{star}_i} - x_{\text{new}_i})^2 + (y_{\text{star}_i} - y_{\text{new}_i})^2 \right] \Big/ \sigma_i^2, \tag{9}$$

where

$$\sigma = 1/(\text{magnitude of signal}). \tag{10}$$

The magnitude of the signal is the variance at the peak position. The sum in Eq. (9) goes over all tubes in which stars are detected for a complete night of data taking. Applying the χ^2-minimization to a set of stars (e.g. a complete night) rather than to single stars guarantees that most sections of the mirror are covered by data points. This minimizes systematic effects from single stars only seen in one of four quadrants, which lead to biases especially in the tilt parameter.

In practice, we do not expect the tilt parameter P_2 to be very large, so instead of using the full rotation matrix as shown in Eqs. (7) and (8), linear approximations for the trigonometric functions are sufficient.

Not all of the tracks represent good data. There are occasional gaps in the track caused by clouds passing over the star or downtime of the detector. Electronic noise, for example very large spikes, is sometimes not successfully filtered by the second difference method. This causes clustering of the maxima of the tubes around certain points in time and space. As stars have a distinct velocity when traversing a mirror, these clusters can be easily removed. Also, we include algorithms to check on the length of pieces of tracks with gaps in them. Any clustering and any pieces of track that are too short (<3°), or have large gaps (>6°), are removed from the fit.

We use this method to find the parameters P_i for 28 days of excellent weather conditions between 19 March 2001 and 25 September 2001. We calculate the parameters for each day of this period to analyze the stability of the method, and we derive a total P_i by making a χ^2-minimization of the whole 28 day data set. This automatically weights the days by the number of detected stars and the track lengths. Fig. 6 shows the stability of the offset parameters P_3 and P_4 as a function of the Julian day for a mirror which shows a considerable shift in x and y.

For most of the mirrors, the correction parameters are small. There is no obvious tilt (P_2) in any of the mirror/camera systems, but several tubes show an offset in the horizontal (P_3) or vertical (P_4) direction, for a few mirrors as large as 0.8–1.5 cm, corresponding to angular errors of 0.2–0.3°.

The dashed line in Fig. 7 shows the distribution of the P_i, obtained for single days for all mirrors with sufficient data. The distribution reflects both the errors in the mirror pointing and the statistical error of the method. Once the mirror pointing is corrected based on the whole data set, further χ^2-minimizations will result in P_i distributions without systematic biases due to mirror misalignment. Assuming the single uncertainties are uncorrelated, the width of the distribution can now be

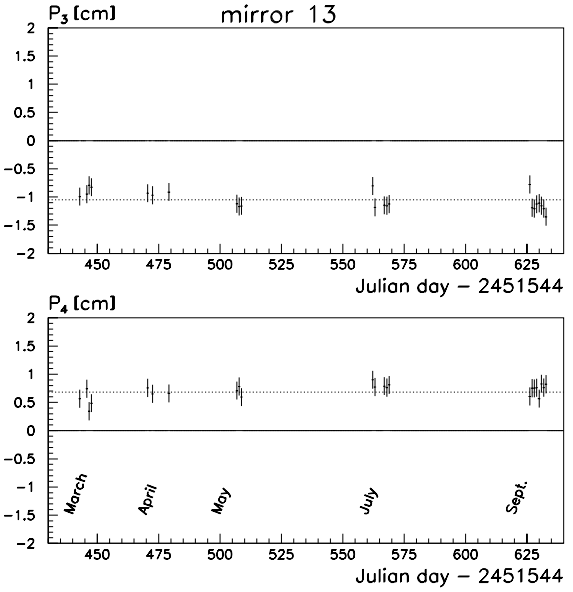

Fig. 6. The offset parameters P_3 and P_4 as a function of Julian day for mirror 13. The dotted lines show P_3 and P_4 estimated from the complete data set.

interpreted as the statistical error of the method if we used a single day's data for the minimization. The resulting distribution after a correction of the mirror positions is shown as the solid line in Fig. 7. An estimate of the accuracy of the method based on this distribution is summarized in Table 1.

If we artificially introduce errors in the mirror pointing, the distribution of the P_i for individual days shows the same spread about the P_i value needed to correct for the error. Further checks also show that the parameters P_i are largely independent. If we introduce artificial errors in more than one of the parameters of a mirror, the method correctly finds the parameters P_i which compensate for the errors.

6. Spot shape

Air fluorescence detectors measure the fluorescence light produced by the passage of an air shower. The variance of the light as a function of the atmospheric depth reflects the longitudinal

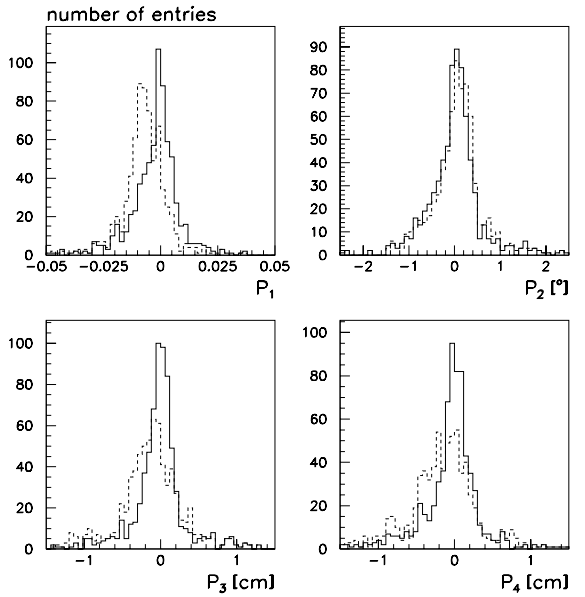

Fig. 7. The distribution of the parameters P_i obtained from single day χ^2-minimizations for all mirrors (- - -). A further χ^2-minimizations applied to the corrected mirror positions gives P_i distributions which reflect the statistical uncertainty of a single day minimization (—).

Table 1
Accuracy of the star pointing method for the four parameters of the χ^2-minimization

Parameter	Accuracy
Scale parameter P_1	$0.006/\sqrt{n}$
Tilt P_2	0.05 rad$/\sqrt{n}$
Horizontal offset P_3	0.16 cm$/\sqrt{n}$
Vertical offset P_4	0.16 cm$/\sqrt{n}$

n is the number of days.

development profile of the air shower. Integrating the shower development profile, one can reconstruct the energy of the shower. The light collected from any given point in the field of view forms a finite spot on the face of the tube cluster. To first order, the image of a point source has a Gaussian-shaped intensity distribution. However, the size and shape of the spot is influenced by imperfections of the mirror surface, and with increasing distance from the optical axis spherical aberrations become an issue. Depending on the location, the size of the spot will be larger than the geometric size of the photo cathode of a single tube and the light is spread over several tubes. In addition, a certain amount of light will be lost because of the physical gap between neighboring tubes. For a correct energy estimation, it is crucial to recover all the light which reaches the detector. This requires detailed knowledge of the response of the tubes to the light collected by the mirror.

A bright star with its precisely known position provides an almost perfect point source. By measuring the distribution of light from a star, we can find the changing responsiveness across the tube cluster and analyze the spread of the light over neighboring tubes. In principle, these results can be directly used to correct the amount of light measured by the tubes in real cosmic ray event reconstruction. However, the number of bright stars that are suited for this analysis is not large enough to cover a whole mirror with a fine enough grid of positions. To mimic the response for tubes on any given position on the cluster, we have to perform a "ray tracing" simulation procedure. The details of the detector including the imperfections of the mirror, distance between the cluster and the mirror, tube positions in the cluster and the response of the photo cathode as a function of the location in a tube, have been incorporated. The results from star measurements described below are used to check and adjust this simulation procedure.

Before we analyze the effects on the spot shape that arise at large distances from the mirror axis, we study the shape of the signal near the center of the mirror. Here, the spot shape can be expected to be symmetric. Fig. 8(a) shows the variance of a tube as a function of the angular distance to a bright star. The tube is close to the mirror center, and the spot shape can be described by a Gaussian with $\sigma = 0.30° \pm 0.01°$. Close to the edge of the mirror, the shape is no longer a symmetric Gaussian but shows a considerable tail (Fig. 8(b)).

On its path across the mirror, the star is observed by tubes at increasing distance to the mirror axis. At every given snapshot time we add the variances of all tubes in a 2° neighborhood of the exact star position. This sum of the variances, after accounting for background, is the total amount of light detected from the star (or the *total signal*).

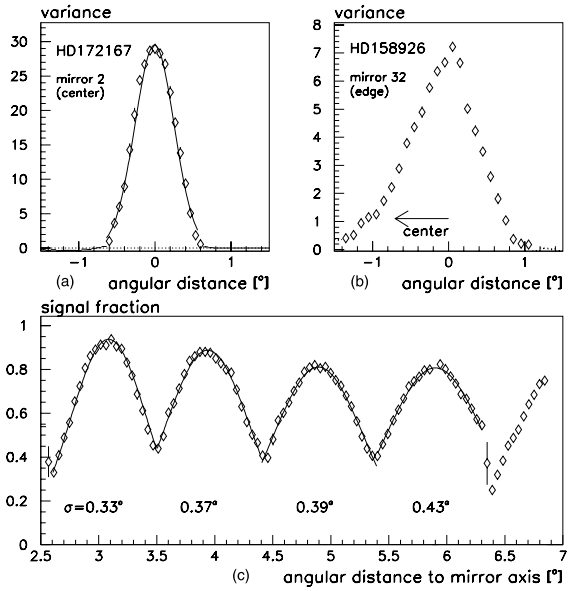

Fig. 8. Variance of a tube (a) near the mirror center and (b) close to the edge of the mirror as a function of the distance between the passing star and the tube center (the arrow indicates the direction to the mirror center). (c) Variance of tubes along the track of a star vs. distance from the center of the mirror. The variances are given as fractions of the total variance, i.e. the sum of the variances of all tubes near the image of the star.

For this analysis, the background level of each tube used in the sum has to be subtracted. We estimate the background level for individual tubes and times by averaging the variance level and slope in a 200 s interval centered 500 s before and after the star peak. The background is then smoothed over several snapshots to decrease the statistical error.

Fig. 8(c) illustrates how the width of the spot increases for a typical star while it moves further away from the mirror axis. The fraction of the total light seen by an individual tube is fitted by a Gaussian, and the width increases from 0.33° at 3° angular distance from the axis to 0.43° at 6°. Closer to the edge of the camera, the shape becomes more and more asymmetric.

The total amount of light depends on the altitude of the star and the position of the image of the star on the camera. The first effect is a consequence of atmospheric absorption. The atmospheric depth increases with decreasing altitude, which leads to a decrease in the total collected light at lower altitudes. The total collected light A as a function of altitude δ can be approximated by $A(\delta,\alpha) = A_0 e^{-\alpha/\sin\delta}$, where α is a parameter which depends on the atmospheric conditions. Typical values for α on clear nights are 0.4–0.5.

However, the total collected light vs. time shows significant structure on a shorter time scale, mainly caused by the small gaps between sensitive areas of adjacent photomultiplier tubes. To estimate the amount of light "lost" in these gaps we analyze a star with a nearly horizontal track. Effects from changes in the atmospheric depth are therefore negligible. Fig. 9(a) shows the track of a star in altitude and azimuth with respect to the mirror axis. The positions of the tube centers are indicated. The altitude of the star changes only by $\simeq 0.5°$, while the star covers more than 8° in azimuth. On its path the distance between the star image on the cluster and the center of the closest

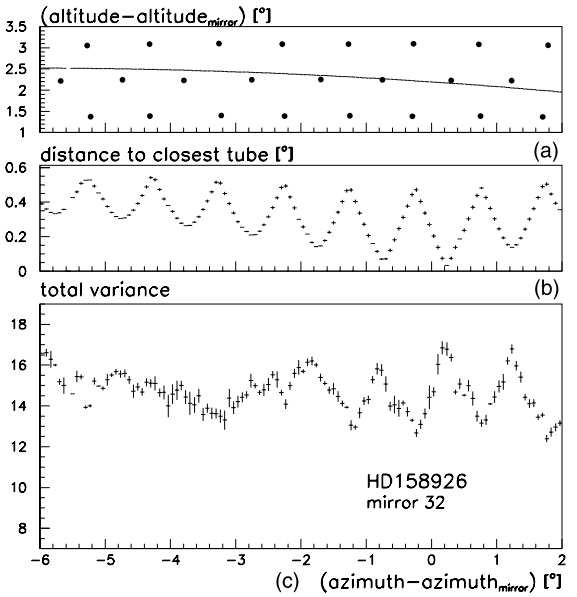

Fig. 9. Effect of gaps between the photomultiplier tubes on the total variance detected in a mirror for a nearly horizontal star track: (a) shows the star track in altitude and azimuth, with the tube center positions indicated by dots, (b) shows the distance of the star to the closest tube and (c) the sum of the variances of all tubes in the neighborhood of the exact star position as a function of azimuth.

tube takes on all possible values from 0.5° to ≃0° (Fig. 9(b)). Fig. 9(c) shows the sum of the variances of all tubes in the neighborhood of the star image vs. azimuth, illustrating the loss of light in the gaps between tubes. At the star's closest approach to a tube, the total collected light reaches its maximum value of ≃17. If the center of the image is between tubes, minimum values of ≃13 are possible, indicating that more than 25% of the total light is lost in the gaps.

Bright stars also enable us to study how the total light collected from of a point source is distributed over several tubes as a function of the position on the mirror. As an example, the fraction of the total light of a bright star as seen by tubes on or near its track as a function of time is shown in Fig. 10. At any given time, the total light is spread over two or more tubes. This often produces a typical triangular image, with the closest tube seeing the main fraction of the light. The two adjacent tubes on the prolongation of the star track on the hexagonal pattern share the remaining fraction. A typical example is the spread of the collected light at times >18000 s in Fig. 10. The signal in the closest tube (filled dots) slowly decreases with the star passing over the tube. Two tubes in the next row (open diamonds and filled triangles) observe the remaining fraction of the light.

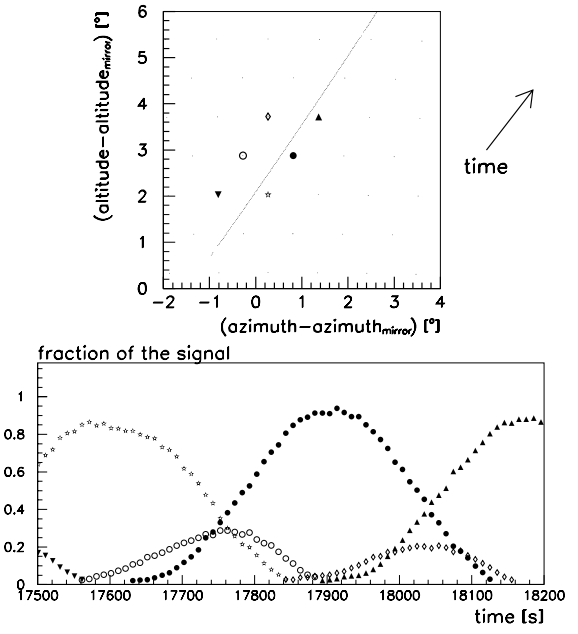

Fig. 10. Contribution of individual tubes along the path of a bright star to the total light, i.e. the sum of the variances of all tubes near the star image, in fractions of the total light. The upper plot shows the star track in altitude and azimuth, with tube positions indicated by symbols, and the lower plot shows the fraction of the total light seen by the corresponding tubes.

Time series as shown in Fig. 10 allow an evaluation of the distribution of light over the tubes for a point source at a given position on the mirror. The error of the method is dominated by the error of the background subtraction. Because marginal peak signals lead to large uncertainties in the estimation of the total signal, only bright stars with peak variances larger than 15 photoelectrons are suited for this analysis. Errors mainly stem from tubes sharing a small fraction of the total light which can not be accurately estimated as it is smaller than the statistical error of the background. The restriction to bright stars implies that not all sections of each mirror can be analyzed. However, the method supplies the necessary input for ray tracing simulations and provides an independent test of the assumptions on the signal spread implemented in the simulation.

7. Conclusions

Stars in the field of view of air fluorescence detectors are undesired sources of detector noise. Photomultiplier tubes along the track of a star see a rate increase with a typical duration and shape. As stars are point-like sources with a very accurately known position, they can be turned into calibration tools to monitor the geometry and optics of the mirror/camera units on a daily basis. Using UV bright stars, we have analyzed the pointing accuracy of the 42 mirrors of the HiRes 2 air fluorescence detector and evaluated the spot shape as a function of distance to the optical axis.

Future work will include a more detailed study of the star intensity as a function of star elevation. The attenuation of star light with increasing atmospheric depth may provide valuable cross-checks on the atmospheric conditions during data taking. By continuously monitoring which bright

stars in the field of view are actually observed and which stars are not, we can estimate for any given data set which parts of the sky are obscured by clouds.

Acknowledgements

Parts of this analysis were performed during the 2001 REU (Research Experience for Undergraduates) program at Columbia University's Nevis Laboratories which is supported by the National Science Foundation (NSF) under contract number NSF-PHY-0097605.

The HiRes project is supported by the NSF under contract numbers NSF-PHY-9322298, NSF-PHY-9904048, NSF-PHY-9974537, by the Department of Energy Grant FG03-92ER40732, and by the Australian Research Council. The cooperation of Colonel E. Fisher, US Army Dugway Proving Ground, and his staff is appreciated.

References

[1] N. Chiba et al., Nucl. Instr. Meth. A 311 (1992) 338.
[2] R.M. Baltrusaitis et al., Nucl. Instr. Meth. A 240 (1985) 410.
[3] J. Boyer, B.C. Knapp, E.J. Mannel, M. Seman, Nucl. Instr. Meth. A 482 (2002) 457.
[4] G.I. Thompson et al., Catalog of Stellar Ultraviolet Fluxes, The Science Research Council (1978).
[5] M.A. Mariscotti, Nucl. Instr. Meth. 50 (1967) 309.
[6] D.R. Bergman et al., Determining the alignment of HiRes optics using a CCD camera, Proceedings of the 27th International Cosmic Ray Conference, Hamburg, Germany, HE 142, 2001.